Nuclear Instruments and Methods in Physics Research A 711 (2013) 124–131

Contents lists available at SciVerse ScienceDirect

Nuclear Instruments and Methods in Physics Research A

journal homepage: www.elsevier.com/locate/nima

RF strip-line anodes for Psec large-area MCP-based photodetectors

Hervé Grabas [a,1], Razib Obaid [a], Eric Oberla [a], Henry Frisch [a,*], Jean-Francois Genat [a,2], Richard Northrop [a], Fukun Tang [a], David McGinnis [b], Bernhard Adams [c], Matthew Wetstein [c,3]

[a] Enrico Fermi Institute, University of Chicago, United States
[b] European Spallation Source, Lund, Sweden
[c] Argonne National Laboratory, United States

ARTICLE INFO

Article history:
Received 7 September 2012
Received in revised form
23 January 2013
Accepted 29 January 2013
Available online 8 February 2013

Keywords:
Photodetector
Anode
Microstrip
Microchannel plate
Analog bandwidth
Large-area detector

ABSTRACT

We have designed and tested economical large-area RF strip-line anodes made by silk-screening silver onto inexpensive plate glass, for use in microchannel plate photodetectors to provide measurements of time, position, integrated charge, and pulse waveform shapes. The 229-mm-long anodes are modular, and can be attached in series for economy in electronics channel-count. Measurements of the anode impedance, bandwidth and cross-talk due to inter-strip coupling are presented. The analog bandwidth, a key determinant of timing resolution, decreases from 1.6 GHz to 0.4 GHz as the anode length increases from 289 mm to 916 mm.

1. Introduction

The development of large-area (m^2) photodetectors with time resolutions of picoseconds (10^{-12} s) and sub-millimeter space resolutions would open new opportunities in many areas, including collider detectors, rare kaon experiments, and neutrino experiments in particle and nuclear physics, X-ray detection at light sources, and time-of-flight positron emission tomography (TOF-PET) [1,2]. Micro-channel plate photomultipliers (MCP-PMTs) [3] have previously been shown to provide space resolutions of a few microns [4], time resolutions down to 5 psec [5], and risetimes as short as 60 psec [6]. MCP-based detectors with bandwidths in the GHz regime are predicted to give sub-psec time resolutions [2,7].

Capacitively-coupled anodes have been developed with good space and time resolutions for a number of applications [8–11]. In this paper we describe the design and testing of economical strip-line anodes [12] with RF analog bandwidths in the GHz range and lengths up to 92 cm being developed by the LAPPD Collaboration [13] for large-area MCP-based photodetectors. The design described here was set at a point in the parameter space of cost, time resolution, space resolution, area covered per channel, and channel density appropriate for applications requiring large area, low cost, and modest resolutions (<10 psec in time and 400 μm in space for signals from charged particles and high-energy photons, and <100 psec and 2 mm for single visible photons). A different optimization of the design would allow the construction of higher performance anodes for applications that require better resolution [14].

The LAPPD design is based on an MCP consisting of a 20×20 cm^2 (8 in. $\times$ 8 in.) capillary glass plate with 20-μm pores [15], functionalized with resistive and emissive layers using atomic layer deposition [16–19]. This method allows separately optimizing the three functions performed by a conventionally constructed MCP: providing the pore structure, a resistive layer for current supply, and the secondary emitting layer. In addition, the micro-pore substrates are a hard glass, providing a more chemically stable platform and improved mechanical strength.

The structure of the LAPPD MCP-PMT vacuum photodetector is shown in Fig. 1 [13]. A photo-cathode is deposited on the vacuum side of the top window, which is followed by an accelerating gap for the initial photo-electron, a pair of 20×20 cm^2 MCPs in a chevron geometry that amplify the single electron by a factors up to 5×10^7, a gap after the output of the second MCP, and an anode plane that collects the amplified pulse of electrons. Incident photons are converted into electrons by the photo-cathode.

* Corresponding author. Tel.: +1 773 702 7479; fax: +1 773 702 1914.
E-mail address: frisch@hep.uchicago.edu (H. Frisch).
[1] CEA/IRFU/SEDI; CE Saclay-Bat141 F-91191 Gif-sur-Yvette CEDEX, France
[2] Present address: LPNHE, CNRS/IN2P3, Universités Pierre et Marie Curie and Denis Diderot, T33 RC, 4 Place Jussieu, 75252 Paris CEDEX 05, France.
[3] Joint Appointment with the Enrico Fermi Institute, University of Chicago.

0168-9002/$ - see front matter © 2013 Elsevier B.V. All rights reserved.
http://dx.doi.org/10.1016/j.nima.2013.01.055

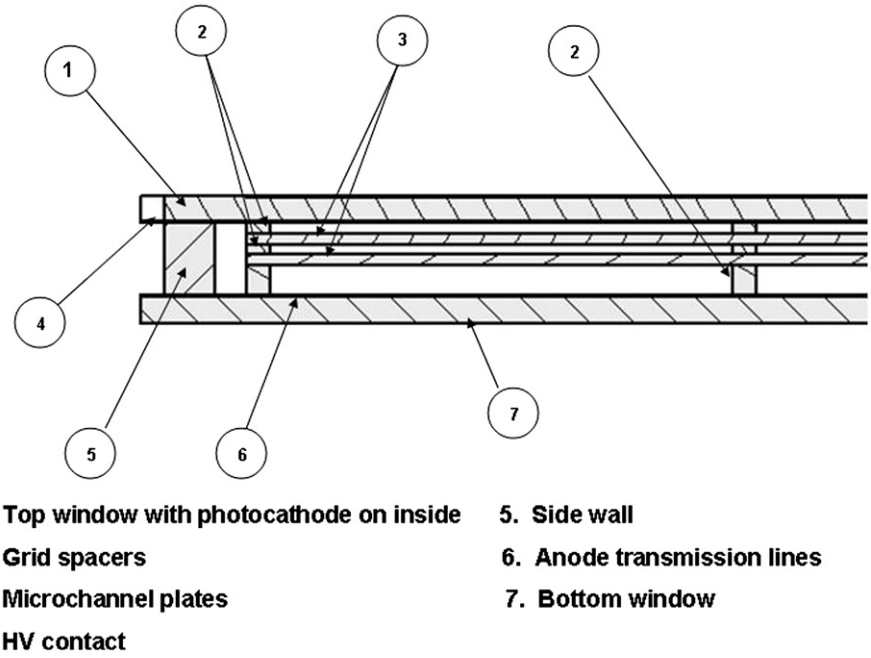

Fig. 1. The basic structure of the glass LAPPD MCP-PMT detector. The sealed vacuum tube consists of a top window with the photocathode on the inner surface, an accelerating gap for the initial photo-electron, a pair of 20-cm-square MCPs in a Cherenkov geometry that amplify the photo-electron by factors up to 5×10^7, a gap after the output of the second MCP, and the anode that collects the exiting 'cloud' of electrons. The package is less than 15 mm thick.

Each of these photo-electrons is accelerated into a pore of the micro-channel plate where it causes a cascade by the process of secondary emission. The electrons emerging from the far ends of the pores are then accelerated towards an anode where they are collected. Measuring the time and position of the anode pulse gives both time and space resolution information on the incoming particle [8–11]. The intrinsic granularity is set by the pores; there are approximately 80 million pores in one of the 8 in. 20-μm pore Incom glass substrates in the baseline LAPPD design [15]. The granularity of the readout is set by the anode pattern, which is quite flexible, allowing many possible patterns and channel sizes [20].

1.1. Picosecond timing measurement and spatial resolution

Due to the small feature size of the amplification stage, MCP-based photodetectors are intrinsically very fast, with risetimes measured down to 60 psec [6]. MCP's are also spatially homogeneous, so that the risetimes are equally fast everywhere on the photodetector area. An essential step in developing fast photodetector systems with areas measured in meters-squared is thus the development of a large-area inexpensive anode with an analog bandwidth capable of retaining the intrinsic speed of the pulse. Parametric extrapolations with higher system analog bandwidth, using sampling rates and signal-to-noise ratios already achieved, predict time resolutions well below 1 psec [7].

The potential exists for even faster MCP risetimes by using smaller pore sizes enabled by the stronger glass of the borosilicate substrate, higher secondary emission yield (SEY) materials at the top of the pores, and ALD-based discrete dynode structures inside the pores [21].

Spatial resolution depends as well on the small feature size of the MCP pores, which provide an intrinsic resolution on the order of the size of the pore. Measurements with spatial resolutions down to 5 μm have been reported using strip-line anodes [4]. The RF-stripline anode design presented here, however, is focused on applications where excellent time resolution is needed over large areas.

1.2. Outline

A brief outline of the paper as a guide to the reader follows. The calculation of time and position using the time-of-arrival of the pulses at both ends of the strips of the transmission line anode is presented in Section 2. Section 3 describes the anode construction of inexpensive plate glass and silk-screened silver strips. The techniques and test setups used to make the measurements of bandwidth, impedance, attenuation, and cross-talk in the frequency domain are described in Section 4. Sections 5–7 present measurements and predictions of anode impedance; bandwidth; and attenuation and cross-talk, respectively. Section 8 summarizes the conclusions.

2. Using RF strip-line anodes and wave-form sampling to measure position, time, and properties of the pulses

The charge cloud of the electrons emerging from the pores of the MCP stack holds both the space and time information generated by the initial photon or relativistic charged particle impinging on and traversing the window [22]. In the LAPPD design, shown in Fig. 1, the charge cloud propagates towards an array of multiple strip-lines. On each strip-line, the pulses created by the charge excitation propagate in opposite directions to the ends of the line, where they are digitized by waveform sampling. From the digitized pulses at each end one can determine the time, position, total charge, and pulse shape of the impinging particles. The spatial location of the charge along the strip direction is determined from the difference in times measured on the two ends of a strip. The one-dimensional nature preserves the excellent space resolution but with many fewer channels of electronics than with a two-dimensional pixel array. In the transverse direction the resolution is determined by the strip spacing in the present one-dimensional implementation of the anode [23]. The time of the deposited charge is given by the average of the times at the two ends of the strip.

The precision of both time and space measurements depends on four parameters of the pulses that arrive at the end of a strip [2,7]: (1) the signal-to-noise ratio; (2) the risetime of the pulse; (3) the sampling frequency of the digitization; and (4) fluctuations in the signal itself. The risetime of the detected pulse will be limited by the analog bandwidth of the strip-line for applications with low-cost large-area readout [2,20]. It is the analog bandwidth of the strip-lines that is the focus of this paper.

The glass package design uses the MCP internal components for both the DC HV current supply and the fast signal generation. In particular, the anode plane of RF strip-lines provides both the signal virtual ground and the HV DC ground, as shown in Fig. 2. Multiple tiles can be daisy-chained by bridging the strip-lines on one tile to the next, forming a continuous strip-line. Each strip-line is terminated in 50 Ω at each end of a tile-row, where the read-out electronics is located.

The time-of-arrival information at each end of a strip is extracted from the leading edge, the peak, and a portion of the trailing edge of the pulse just beyond the peak, at each end of the strip [2]. The measurement of relative times-of-arrival at the two ends benefits from the inherent correlation between the shapes of the pulses at each end of the strip. Using a commercial MCP excited by a laser as a source, we have measured a relative resolution of 2 psec on a 5 in.-ceramic–substrate strip-line anode [24]. Using a pair of the LAPPD 8 in. MCPs [25] and a 229-mm-long 30-strip glass anode (see the left-hand panel of Fig. 3), we have measured a relative resolution of <5 psec [25].

The difference in times-of-arrival between the pulses recorded at the two ends of the strips provides a measurement of the position of the incident radiation in the direction along the strips. The anodes used here have a nominal impedance of 50 Ω and a measured propagation velocity of $0.57\pm0.07c$ (170 ± 20 μm/psec). The correspondence between the position resolution δx and the time resolution of the pulse δt is given by $\delta x \approx 1/2\delta t \times v$, where v is the propagation velocity.

The position in the direction transverse to the strips is measured by simultaneously digitizing the signals on every strip in the one-dimensional anode design presented here. The strip or strips closest to the position of the incident radiation will carry the largest signal. The neighboring strips carry signals induced capacitively and inductively (see Section 7). While energy is transferred from the central strip into the neighboring strips, not all information is lost, as the neighboring strips are digitized. In the ideal limit of zero noise the information can be completely recovered in the case of a single hit.

A benefit of the wave-form digitization readout is that it gives the equivalent of an oscilloscope trace for both ends of each of the strip-lines, allowing the extraction of amplitude, integrated charge, shape, and separation of overlapping or near-by pulses ('pile-up') [2]. The measured shape will depend on the analog bandwidth, cross-talk, attenuation, and signal-to-noise ratio of the system, and will thus depend on the position of the incident excitation for large systems. In addition, care has to be taken in impedance matching the detector to the electronics to avoid losses from reflections at interfaces.

Ref. [2] contains a comparison of methods to extract the time-of-arrival of a pulse. A study of the benefit of using a more sophisticated fit to the pulse shape is presented in Ref. [26]. Waveform sampling allows extracting much more information than just the time, however; a fit to a template shape allows the extraction of the amplitude, integrated charge, a figure-of-merit for the goodness of fit to the shape, and possible separation of

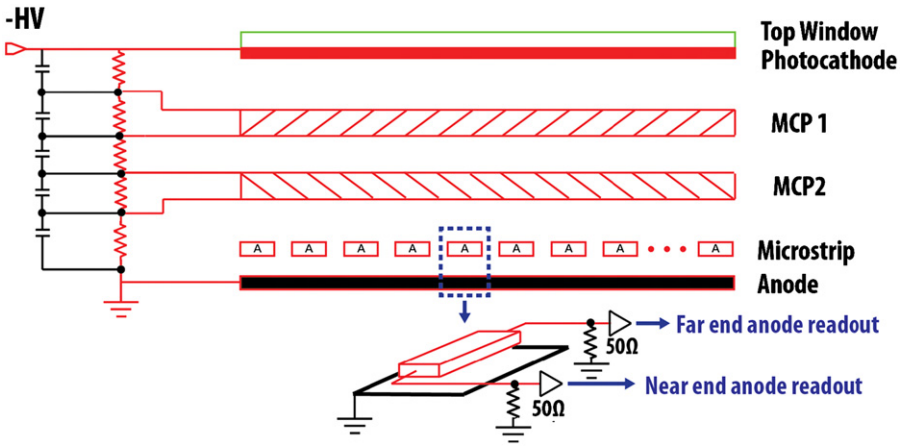

Fig. 2. The equivalent electrical HV and signal circuits of the strip-line anode. The silver strip-lines are fired onto the top surface of the glass plate that forms the bottom of the tile package. The sealed tiles (see Fig. 1) sit on a copper sheet, which acts as the ground plane for the strip-line. Each strip-line is terminated in 50 Ω at each end.

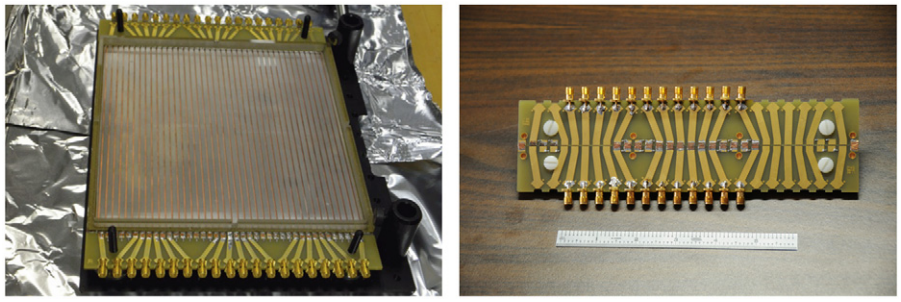

Fig. 3. Left: a single tile with a 229.1 mm-long 40-strip anode. The anode strips are connected at both ends to the fanout cards used for testing. Right: a 'zero-length tile' consisting of a pair of fanout cards, used to characterize the measurement system with no tile.

nearby or overlapping pulses. Algorithms such as these can be implemented in FPGA-based processors located close to the waveform digitization front-end, allowing only the higher-level parameters of the pulse to be transmitted to the next level of analysis [27].

3. Anode design and construction

The aim of the LAPPD project is to develop a large-area economical photodetector with good space and time resolution, low electronics channel count and power, and low noise. We have developed a mechanical design based on inexpensive commercial float glass [28]. This glass can be water-jet cut, and so many aspects of the construction are widely available and standard in industry. In this section we describe the application of these principles to the design and construction of the anode.

3.1. Choice in anode parameter space for the proof-of-concept detector

The LAPPD project was started in 2009 with the goal of developing a commercializable module in 3 years. Choices had to be made for the initial parameters for proof-of-concept, with the understanding that after the 3-year R&D phase, modules for specific applications would be designed with optimized parameters. The parameters of the initial design described here were chosen to be appropriate for applications requiring large area, low cost, and modest resolutions. The flexibility of the design, however, should allow optimizations for very precise timing at colliders and other applications.

The initial choice of an 8 in.-square (200 mm) module was made to be significantly larger than available MCP-PMT's but sized to widely-available vacuum components and light enough to be handled by vacuum transfer equipment. In addition, a 200-mm anode is long enough to be treated as a transmission line for typical MCP risetimes.

The glass package as well as the anode glass substrate were chosen for cost considerations—Borofloat glass [28] is widely available and inexpensive. Evaporation and sputtering to form the metalized strip-lines on the surface of the anode were successfully tried; however, the silk-screening of silver-loaded ink [29] proved significantly less expensive with a very fast turn-around, as a silk-screen is much more easily produced than a mask, and the silk-screening process is entirely mechanized and in air rather than in vacuum. The high-frequency behavior of the glass and silk-screened silver are adequate to handle the bandwidth of the present generation of 20-μm pore MCP's.

The choice of the anode strip width was set by a choice of a 50 Ω strip impedance. This is determined by the thickness of the glass anode substrate (2.75 mm) and the dielectric constant of the glass [28].

The choice of the gap spacing between the anode strips depends on competing considerations. The cross-talk between strips decreases with gap size. However, a large gap provides a high-resistance area on which charge could accumulate, possibly leading to hysteresis or breakdown at high rates. A larger gap size diminishes the electronics channel count but increases the transverse spatial resolution [23].

3.2. The single tile anode

The LAPPD design is modular, with the unit module being a sealed planar glass vacuum tube with an 8 in. (200 mm)-square active area, called a 'tile'. The metal strips that form the anode for the tile are formed by the inexpensive technique of silk-screening a silver-based ink [29] onto the glass plate, and then firing the plate at high temperature [30] to burn off the volatiles, leaving behind the silver traces. The thickness of the silver trace is typically 10−15 μm. The dimensions of the glass plate, 229.1 mm by 220.0 mm, are set

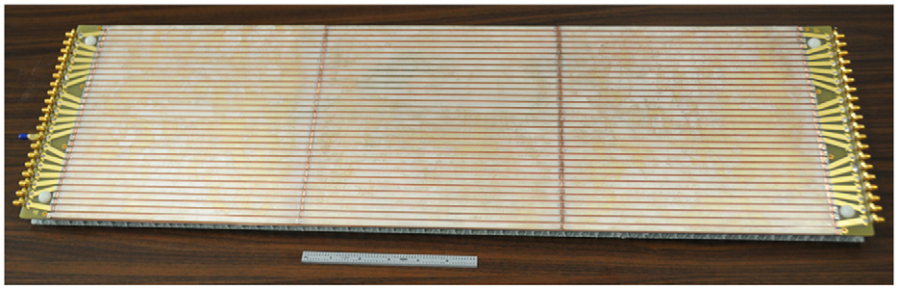

Fig. 4. The 3-tile anode used to measure bandwidth, attenuation, and impedance as a function of anode strip length. The connections between anode strips on neighboring tiles have been made by soldering small strips of copper to the silver silk-screened strips on the glass.

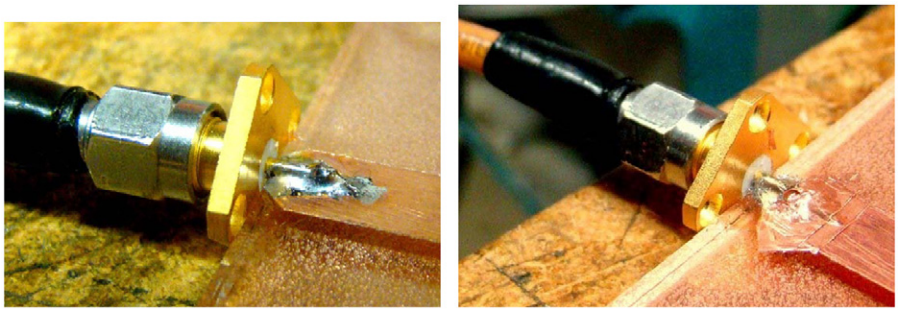

Fig. 5. The geometry of the coupling between the coaxial cable from the pulse generator to the anode strip before modification (left), and after impedance matching with copper tape (right).

by the design of the 8 in.-square MCP-PMT active area. A single tile is shown in the left-hand panel of Fig. 3; the 'fanout' cards used for measurements with the pulse generator, oscilloscope, and network analyzer are shown in the right-hand panel.

Two anode strip patterns have been tested, one with 30 strips and the other with 40, both with a 50 Ω target impedance. The 40-strip anode was an initial design, with small gaps between the strips designed to minimize possible static electric charging of the inter-strip glass, and was well-matched to then-current waveform sampling PSEC-3 ASIC which had four channels, requiring 10 chips per end [31]. The 30-strip anode is matched to a new 6-channel PSEC-4 ASIC [27], halving the chip count to five chips per end. The strip width, strip gap, and plate thickness of the 30-strip anode are 4.62 mm, 2.29 mm, and 2.75 mm, respectively. The corresponding numbers for the 40-strip anode are 3.76 mm, 1.32 mm, and 2.67 mm.

3.3. The multi-tile anode

The strip lines of one tile can be connected in series with the strip lines of a neighboring tile to make a 'tile-row' that shares the common readout on the two ends of the shared multi-tile strip, as shown for a 3-tile tile-row in Fig. 4. The strips on the connected tiles form continuous 50 Ω transmission lines with the ground plane that underlies all the tiles. At each end of a tile-row a fanout card makes the transition to SMA connectors for each strip. Each strip is terminated in 50 Ω, either at the oscilloscope, or, if the SMA connector is left open, with a 50 Ω resistor at the connector.

Measurements were made with anodes consisting of 1, 3, and 4 tiles, where each tile anode is 229.1 mm long. In addition, measurements were made with a 115 mm-long 'half-tile', and, in order to unfold the contribution of the test setup cabling and fanout cards, with the zero-tile configuration, as shown in the right-hand panel of Fig. 3. The connections between anodes are made by hand-soldering small strips of copper to the silver silk-screened strips on the glass, as shown in Fig. 4.

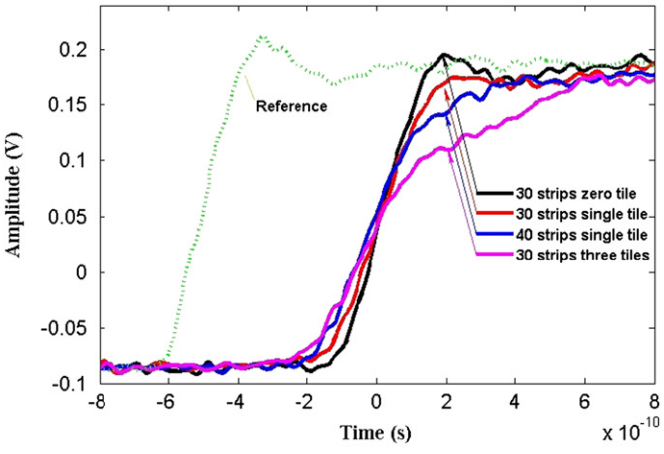

Fig. 6. The anode responses in the time domain to a step-function introduced into one end of a strip in a multi-strip anode. The source of the reference pulse is the calibration output from a Tektronix TDS6154C oscilloscope, which has a risetime of 200 psec and an amplitude of 440 mV (peak–peak). The response curves in the figure were measured with the same oscilloscope.

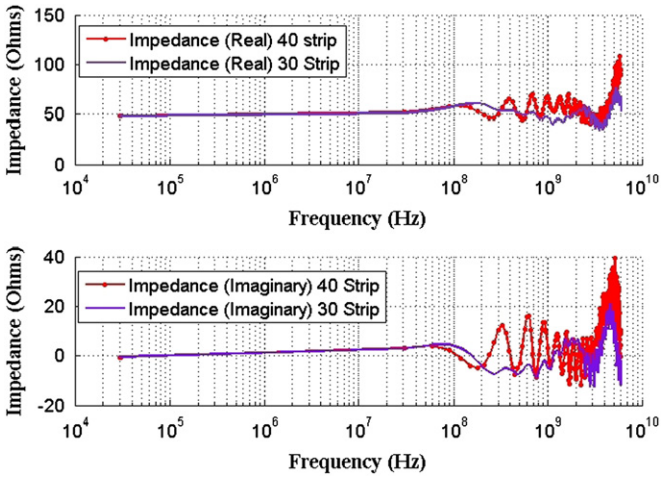

Fig. 7. The measured real (top) and imaginary (bottom) impedance versus frequency for 40-strip and 30-strip silk-screened anodes on a single 229.1 mm-long glass tile base between two fanout cards. The targeted design impedance (top) was 50 Ω.

4. Anode performance

To characterize the bandwidth, attenuation, cross-talk, and impedance of the anodes, signals are introduced via SMA cables to the fanout card at one end of one strip (the 'active' strip), and measurements are made at the far and near ends of that strip and neighbors ('quiet' strips). We describe the details below.

4.1. Impedance matching to the strips

The transition of the $\vec{E}$ and $\vec{B}$ fields between the geometries of the coaxial cable, the SMA cable, and the planar transmission line results in reflections and signal distortion. This can be handled by designing a transition region to match the impedances. Rather than using a full wave simulator to get a theoretical solution, we used an empirical method of tuning by hand while watching the match with a network analyzer. We used adhesive-backed copper tape [32] to construct geometries on the glass substrate. Monitoring the work in the time domain on a network analyzer, one can identify the location of impedance mismatches and make appropriate additions (more capacitance) or subtractions (more inductance) of metal. After optimization, a single shape was adequate for all the strips in the 30-strip tile, as expected.

The left-hand panel of Fig. 5 shows the geometry of the coupling between the coaxial cable from the pulse generator to the anode strip before modification, and on the right, after correction.

4.2. Measurements of pulse rise times

The anode responses to a step-function with a risetime of 200 psec introduced into one end of a strip in a multi-strip anode were measured using the reference fast edge of the calibration output from a Tektronix TDS6154C oscilloscope, as shown in Fig. 6. The 30-strip anode has better bandwidth performance than the 40-strip due to less coupling to neighboring strips. The length of the anode also enters into performance, as the energy transfer to neighboring strips grows with strip length.

4.3. Measuring the bandwidth, attenuation, velocity, and impedance

Measurements of analog bandwidth, attenuation, propagation velocity, cross-talk, impedance, and RF matching were made with an Agilent HP8753E network analyzer [33]. For each tile configuration, signals were introduced from one port on one end of an anode strip via a fanout card, and measured at the far end via a second fanout card. The power on both the near end and the far end was recorded as a function of frequency. The signals on both

ends of neighboring strips were also recorded. The results are given in Sections 5–7 below.

5. Impedance

The impedance of a single strip of width w separated from an infinite ground plane by a glass substrate of thickness h depends on the ratio of strip width to strip-ground plane separation, w/h [34].

In the case of an array of multiple strip-lines, the impedance of the lines is more complicated, as the geometry of the field lines is affected by the adjacent strips. Consequently additional excitation (odd and even) modes exist, modifying the impedance of the single strip-line mode [35–37]. The impedance of the lines is thus not only a function of the w/h ratio but also of the width of the gap between the strips.

Fig. 7 shows the measured real and imaginary parts of the impedance versus frequency for 40-strip and 30-strip silk-screened anodes on a single 229.1 mm-long glass tile base between the fanout cards. The targeted design impedance (real part) was 50 Ω. The impedances are well-matched to the few-GHz bandwidth of the present MCP's. The imaginary part of the 30-strip anode stays relatively small up to the few-GHz region, well-matched to the bandwidth of the present LAPPD 220-mm-square 20-μm pore MCP's.

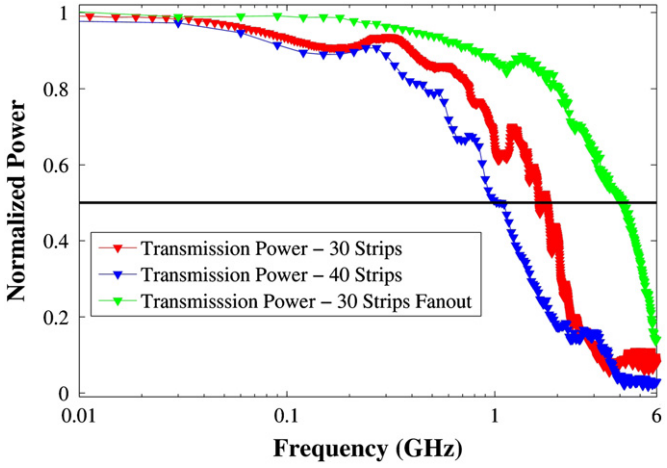

Fig. 8. The normalized power (output power/input power) versus log-frequency for a single 229.1 mm-tile plus fanout cards (288.5 mm) with 30 strips (red, middle trace), 40 strips (blue, bottom trace), and the fanout PC cards alone('zero-tile', in green, top trace). See Fig. 3. The (black) horizontal line represents the 3 db loss level (50% loss in power). (For interpretation of the references to color in this figure caption, the reader is referred to the web version of this article.)

6. Bandwidth

In a strip-line anode geometry, a wave traveling on one strip will also transfer energy to its neighbors due to inductive and capacitive coupling between the strip-lines [36,37]. We have measured the bandwidth over different length strip-lines by connecting the 229.1 mm anode of the tile to a neighboring tile or tiles in series, as shown in Fig. 4.

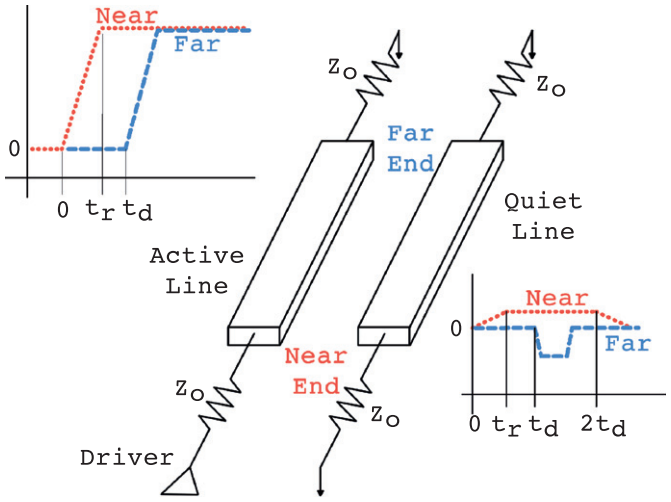

Fig. 10. The mechanism of cross-talk for a positive signal with a linear rising edge [35]. Two adjacent strip-lines are shown; the common ground plane is not shown for clarity. The active line is driven on the near end with a signal pulse of rise-time t_r. At the far end of the active line the same pulse is seen a time t_d later, determined by the length and characteristic velocity of the line. The neighboring line, the quiet line, is coupled to the active line capacitively and inductively by the electric and magnetic fields, respectively. At the near end of the quiet line a positive voltage appears at the start of the signal and persists for $2t_d$. For an inductive coupling, at the far end a negative voltage appears starting at t_d with a width t_r.

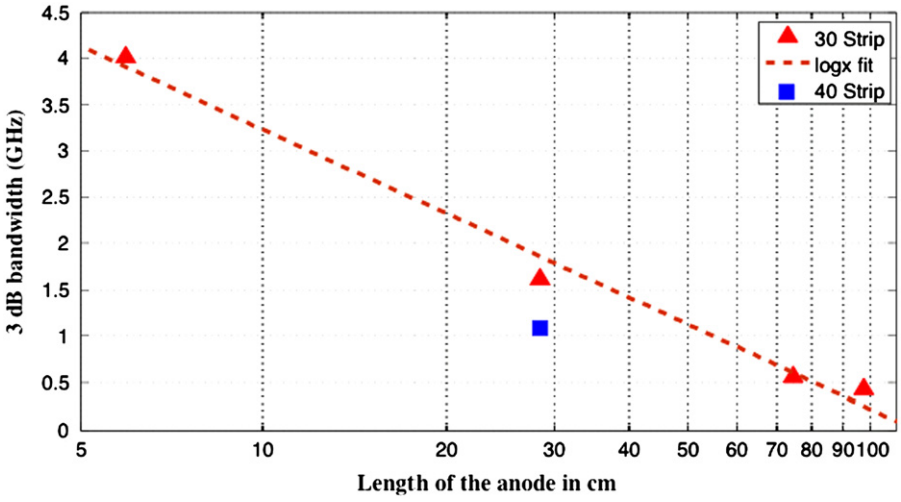

Fig. 9. The bandwidth measured at 3 db loss on the central strip versus the log of the total anode length. The anodes consisted of 3 and 4 tiles in series (746.7 mm and 916 mm, respectively, including the length of the fanout card strips), a single tile (288.5 mm), and only the 2 fanout PC cards connected to each other ('zero tiles'—59.4 mm).

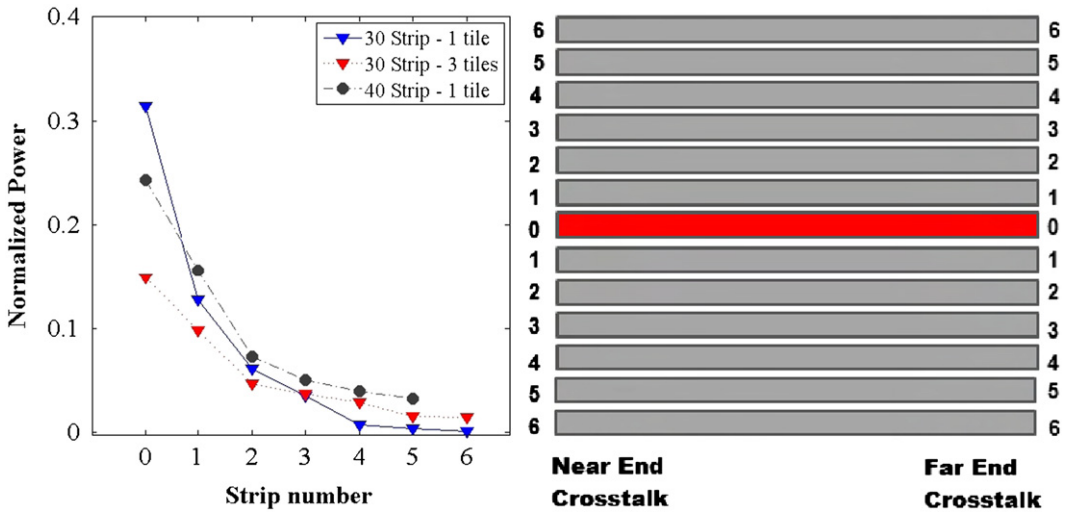

Fig. 11. Comparison of total normalized power summed over all strip-lines for three different anode geometries: a single 30-strip tile (triangles), a single 40-strip tile (circles), and three 30-strip tiles in series. The right-hand panel shows the geometry of the test setup: a signal is input on the near end of the central strip (shown in red) and is detected at the far end. The power is measured on the near and far ends of the neighboring strips. (For interpretation of the references to color in this figure caption, the reader is referred to the web version of this article.)

Fig. 8 shows the measured ratio of output power to input power versus frequency for the three cases of a single 30-strip anode with fanout cards, a single 40-strip anode with fanout cards, and just the fanout cards alone ('zero-tile'). The 30-strip tile has significantly improved analog bandwidth, as well as providing the reduced channel count for the 6-channel PSEC-4 ASIC. No correction has been made for the fanout cards, as they have significantly higher bandwidth than the anodes.

Fig. 9 shows the measured 3-db loss point in frequency for different length anodes. The points shown correspond to the effective length of the fanout card pair alone (59.4 mm), a single tile with fanout cards (288.5 mm), and, in the case of the 30-strip anode, three and four tiles with fanout cards (746.7 mm and 916 mm, respectively). The slope of the exponential fit of the bandwidth (GHz) versus the log of the length in cm is -3.19.

7. Attenuation and cross-talk

The power in a pulse propagating down a strip diminishes with distance due to resistive attenuation in the materials of the strip and coupling to neighboring strips. Two adjacent strip-lines are both capacitively and inductively coupled [35]. A wave traveling down the line induces a signal on its neighbors. This cross-talk, which is the dominant source of loss at high frequencies, produces pulses both at the near and far end of the adjacent strips, as shown in Fig. 10. The degree of acceptable energy loss and signal mixing from one strip to another is application-specific, and can be optimized by changing the strip spacing and impedance, or by using a material with an appropriate dielectric constant.

Fig. 11 shows measurements of the normalized power measured in the driven strip (strip 0) and neighboring strips. A signal is input on the central strip (shown in red) via the fanout card and is detected at the far end. The power is measured on the near and far ends of the strips. The left-hand plot shows the sum of the two ends for each strip. A single 30-strip tile is shown as triangles; measurements on an anode made of three 30-strip tiles in series (see Fig. 4) are represented by squares. A single 40-strip tile is shown as circles.

The single 30-strip tile has the lowest cross-talk, as expected due to its wider spacing than the 40-strip tile, and shorter length than the anode composed of three 30-strip tiles. The effect of cross-talk on pattern recognition will depend on the specific application (specifically occupancy and signal-to-noise), and the implementation of digitization and pattern-recognition algorithms.

8. Conclusions

Anodes for MCP-PMT's with analog bandwidths in the GHz region are predicted to enable sub-psec time resolutions for applications that provide enough initial signal. We have measured the signal properties of a class of inexpensive anodes for use in large-area microchannel plate detectors and other current sources. The strip-line anodes are inexpensively constructed by silk-screening silver ink on widely-available borosilicate float glass. The unit 'tile' anode is 229-mm long; the units can be daisy-chained in series to cover more area with the same electronics channel count. The present LAPPD glass-based design uses 30 anode strips to cover the 220-mm wide anode.

We measure an analog bandwidth of 1.6 GHz on a single tile, and present the bandwidth as a function of the number of tiles for anode strip lines up to 916 mm in length. Results on attenuation, cross-talk, impedance, and signal velocity are also presented. We also describe the techniques and equipment used in the measurements.

Acknowledgments

We thank our colleagues in the Large Area Psec Photodetector (LAPPD) Collaboration for their contributions and support. Particular thanks are due to M. Heintz for critical technical support, G. Varner for RF advice, and R. Metz and M. Zaskowski for machining and mechanical work. J. Gregar (ANL), P. Jaynes (CatI Glass), and E.A. Axtell (Ferro Corporation) provided invaluable advice and technical support on the glass and silver anode application techniques.

The activities at Argonne National Laboratory were supported by the US Department of Energy, Office of Science, Office of Basic Energy Sciences and Office of High Energy Physics under contract DE-AC02-06CH11357, and at the University of Chicago by the National Science Foundation under Grant PHY-1066014.

References

[1] T. Credo (IMSA), H. Frisch, H. Sanders, R. Schroll, F. Tang, Picosecond time-of-flight measurement for colliders using Cherenkov light, in: Proceedings of the IEEE, Rome, Italy, October 2004; Nuclear Science Symposium Conference Record, 2004 IEEE, vol. 1, 16–22 October 2004.

[2] J.-F. Genat, G.S. Varner, F. Tang, H. Frisch, Nuclear Instruments and Methods in Physics Research Section A 607 (2009) 387 arXiv:0810.5590.

[3] J.L. Wiza, Nuclear Instruments and Methods 162 (1979) 587.

[4] A.S. Tremsin, O.H.W. Siegmund, Charge cloud asymmetry in detectors with biased MCPs, in: Proceedings of the SPIE3 4497, San Diego, CA, 2001. A parallel LAPPD effort with a different anode technology, based at the Space Sciences Laboratory, UC Berkeley, is better to suited to applications needing high space resolution.

[5] K. Inami, N. Kishimoto, Y. Enari, M. Nagamine, T. Ohshima, Nuclear Instruments and Methods in Physics Research Section A 560 (2006) 303.

[6] J. Milnes, J. Howorth (Photek Ltd.), Advances in Time Response Characteristics of Micro-channel Plate PMT Detectors. See 〈http://www.photek.com/support/technical_papers.htm〉.

[7] S. Ritt, The Factors that Limit Time Resolution in Photodetectors, Workshop, University of Chicago, Chicago, IL, 28–29 April 2011. See 〈http://psec.uchicago.edu/workshops/〉. Note that of the values needed of the four parameters to achieve a time resolution of 100 fs (the bottom row of the table of extrapolations), we have achieved or exceeded three: sampling rate, noise, and signal size. Only the analog bandwidth falls short at present.

[8] M. Lampton, Review of Scientific Instruments 58 (12) (1987) 2298.

[9] O.H.W. Siegmund, in: J.A.R. Sampson, D.L. Ederer (Eds.), Methods of Vacuum Ultraviolet Physics, second ed.,Academic Press, 1998. (Chapter III).

[10] O. Jagutzki, et al., IEEE Transactions on Nuclear Science 49 (5) (2002) 2477.

[11] J.S. Lapington, J.R. Howorth, J.S. Milnes, Nuclear Instruments and Methods in Physics Research Section A 573 (2007) 243.

[12] The LAPPD geometry of a strip over a ground plane is often called a microstrip transmission line.

[13] The Original LAPPD Institutions Include ANL, Arradiance Inc., The University of Chicago, Fermilab, the University of Hawaii, Muons, Inc, SLAC, SSL/UCB, and Synkera Corporation. More detail can be found at 〈http://psec.uchicago.edu/〉.

[14] For a discussion of the factors that determine time and space resolution in MCP-based detectors, see the talks at: *The Factors that Limit Time Resolution in Photodetectors*, Workshop, University of Chicago, Chicago, IL, 28–29 April 2011. See 〈http://psec.uchicago.edu/workshops/〉.

[15] The glass capillary substrates are produced by Incom Inc., Charlton, MA. See 〈http://www.incomusa.com/〉.

[16] S.M. George, Chemical Reviews 110 (1) (2010) 111.

[17] J.W. Elam, D. Routkevitch, S.M. George, Journal of the Electrochemical Society 150 (6) (2003) G339.

[18] D.R. Beaulieu, D. Gorelikov, H. Klotzsch, P. de Rouffignac, K. Saadatmand, K. Stenton, N. Sullivan, A.S. Tremsin, Nuclear Instruments and Methods in Physics Research Section A 633 (2011) S59.

[19] O.H.W. Siegmund, J.B. McPhate, S.R. Jelinsky, J.V. Vallerga, A.S. Tremsin, R. Hemphill, H.J. Frisch, R.G. Wagner, J. Elam, A. Mane, Development of large area photon counting detectors optimized for Cherenkov light imaging with high temporal and sub-mm spatial resolution, in: Proceedings of the IEEE NSS-MIC, Valencia, Spain, 2011.

[20] Large Area, Pico-second Resolution, Time of Flight Detectors; US Patent US 2007/0187596 A1; 16 August 2007; Inventors: H.J. Frisch, H. Sanders, F. Tang, T. Credo.

[21] J.W. Elam, J.A. Libera, M.J. Pellin, P.C. Stair, Applied Physics Letters 91 (2007) 24.

[22] There are additional effects that make the focusing not exact- see, for example, A.S. Tremsin, J.V. Vallerga, O.H.W. Siegmund, Nuclear Instruments and Methods in Physics Research Section A 477 (2002) 262; A.S. Tremsin, O.H.W. Siegmund, Review of Scientific Instruments 70 (1999) 3282.

[23] The measured transverse resolution for the 229-mm 30-strip anode excited by pulses from the microchannel plate detector is 0.5 mm, comparable to the longitudinal resolution of approximately 0.4 mm; detailed studies of the assembled micro-channel plate detector will be presented elsewhere [38]. We note that in applications such as a collider detector, the unique capability of a system of MCP-PMT's is for psec-level time-of-flight. Much more precise spatial measurements are provided by the central tracking systems, but with much poorer timing.

[24] J.-F. Genat, Development of a Sampling ASIC for Fast Detector Signals, Workshop on Fast Timing, Cracow, Poland, November 2010.

[25] M. Wetstein, B. Adams, A. Elagin, R. Obaid, et al., the LAPPD Collaboration, in preparation.

[26] B. Joly, Optimisation de la résolution temporelle en tomographie par emission de positons dédiée au contrôle de dose en hadronthérapie; Ph.D. Thesis, Université Clermont Ferrand II—Blaise, Pascal, February. 2010. 〈http://tel.archives-ouvertes.fr/docs/00/50/51/29/PDF/BJoly.pdf〉.

[27] E. Oberla, A Fast Waveform-Digitizing ASIC-Based DAQ for a Position & Time Sensing Large-Area Photo-Detector System; Photodet2012, LAL Orsay, France, June 2012.

[28] 〈http://psec.uchicago.edu/glass/borofloat_33_e.pdf#page=28〉; The dielectric constant is 4.6 and the loss tangent is 37×10^{-4}, both measured at 25C and 1 MHz.

[29] Ferro Corp., 251 Wylie Ave., Washington, PA 15301.

[30] Cat-I Glass, P.O. Box 208, S. Elgin, IL 60177.

[31] E. Oberla, A 4-Channel Fast Waveform Sampling ASIC in 130 nm CMOS, TIPP 2011, Chicago, IL, July 2011. Proceedings to be published in Physics Procedia, Elsevier, 2012.

[32] The adding or subtracting of a few-millimeter triangle of copper measurably changes the capacitance and inductance at an interface, and is easily seen with the network analyzer.

[33] Agilent Model HP8753E (6 GHz bandwidth) with Option 010 (Time Domain Option).

[34] I.J. Bahl, D.K. Trivedi, Microwaves (May) (1977) 174.

[35] For an excellent discussion of transmission lines, see E. Bogatin, Signal Integrity Simplified, Prentice-Hall Professional Technical Reference, 2004. Chapter 10 is especially clear on cross-talk in striplines.

[36] R. Harrington, Time Harmonic Electromagnetic Fields, IEEE Press, 1961.

[37] R. Brown, Lines, Waves, and Antennas, John Wiley, New York.

[38] M. Wetstein, B. Adams, A. Elagin, J. Elam, H. Frisch, Z. Insepov, V. Ivanov, S. Jokela, A. Mane, R. Obaid, I. Veryovkin, A. Vostrikov, R. Wagner Alexander Zinovev et al., Nuclear Instruments and Methods in Physics Research Section A, submitted for publication.